Bio-Design and Manufacturing (2024) 7:1035–1052
https://doi.org/10.1007/s42242-024-00318-x

RESEARCH ARTICLE

Photocrosslinkable human amniotic membrane hydrogel for recovery from spinal cord injury

Tao Xu[1] · Changwei Yang[1] · Yang Lu[1] · Heng Wang[1] · Cheng Chen[1] · Yuchen Zhou[1] · Xiaoqing Chen[1]

Received: 4 March 2024 / Accepted: 27 September 2024 / Published online: 12 November 2024

Abstract

The recovery and reconstruction of central nervous system function after spinal cord injury (SCI) is a worldwide problem. The difficulty lies in the feasibility issue of new axons passing through the injured area and the negative effect of scarring after injury. As a biological material, the human amniotic membrane (HAM) has the advantages of protecting nerve growth, inhibiting scar formation, and promoting neovascularization, but its weak physical properties are difficult to apply in treating SCI. In this study, HAMs were first decellularized and then chemically grafted with methacrylic anhydride. Next, the composite was photocrosslinked with gelatin methacrylate to prepare a cross-network biological complex. The final complexes prepared by appeal were used for in vitro and in vivo studies of SCI in rats, separately. In the in vitro experiment, the composite scaffold inherited abundant biological factors from the amniotic membrane and had the physical properties of a hydrogel, thus providing a favorable environment for the growth and development of neurons and blood vessels. In the in vivo experiment, the composite reduced scarring and promoted the growth of new nerves. Overall, the composite scaffolds can stably simulate the extracellular microenvironment in SCI defects, regulate pathological changes, and promote the generation of new neurons. Therefore, decellularized HAM hydrogels are promising biocomposite materials for central nerve repair after SCI.

✉ Xiaoqing Chen
chenxiaoqing@ntu.edu.cn

[1] Department of Spine Surgery, Affiliated Hospital of Nantong University, Medical School of Nantong University, Nantong 226001, China

Graphic abstract

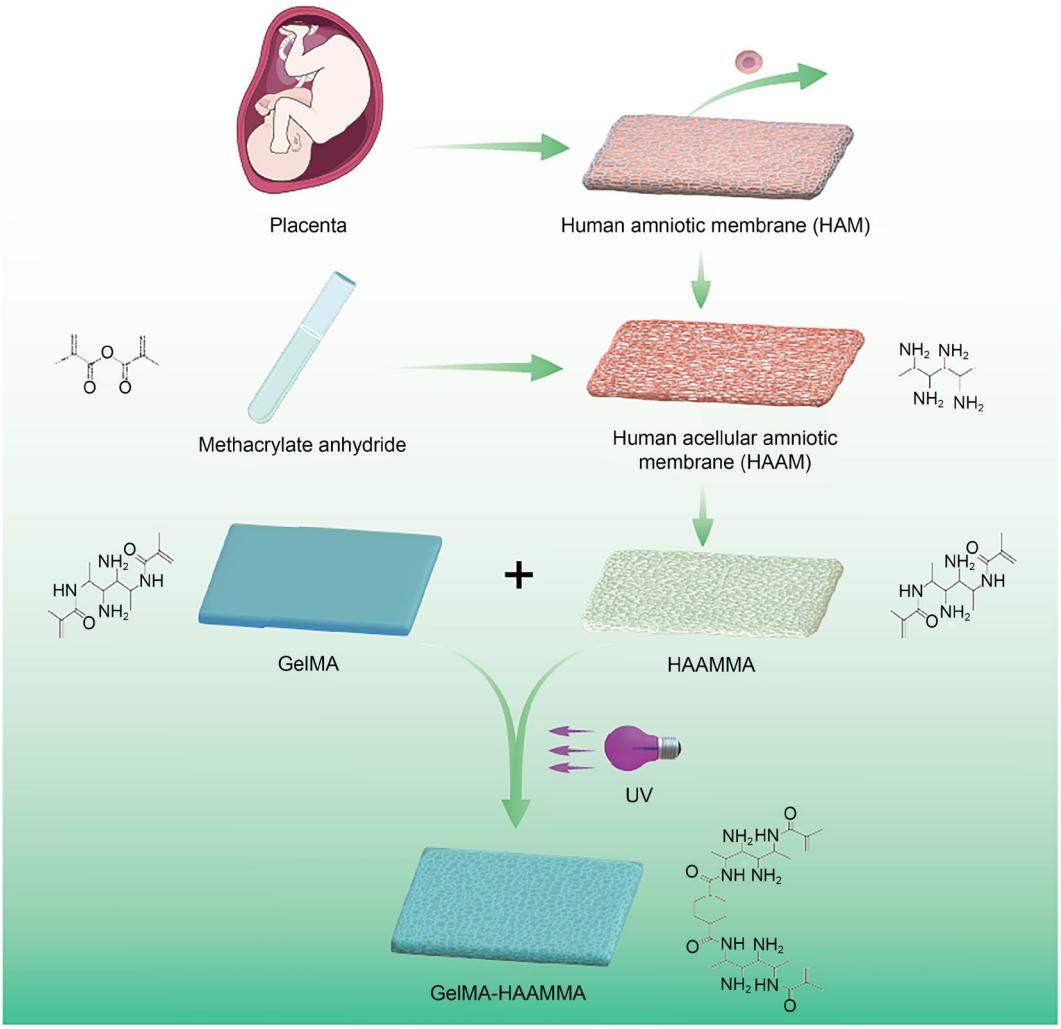

Keywords Spinal cord injury · Nerve regeneration · Human acellular amniotic membrane · Composite hydrogel · Biological materials

Introduction

With the continuous development of tissue engineering and regenerative medicine in nerve injury, many biological functional materials have gradually entered the public vision in recent years. As the thickest basement membrane in the human body, the human amniotic membrane (HAM) has been widely used in corneal transplantation, soft-tissue injury healing, wound dressing preparation, cartilage repair, and tendon repair in ophthalmology [1]. With further research, more scholars have chosen to decellularize HAMs to improve their operability [2, 3]. Moreover, the immunogenicity of decellularized HAMs has been greatly reduced. Human acellular amniotic membrane (HAAM) has been used in cartilage regeneration engineering, vascular regeneration tissue engineering, and other applications due to its excellent biological activity. In many studies, HAAM is usually applied directly to the wound and is sutured in place. Further studies have demonstrated that HAAM can promote wound healing, prevent infection, and reduce inflammation and scar formation [4]. However, as a film with poor mechanical properties, HAAM cannot be effectively used to treat defects caused by spinal cord injury (SCI), limiting the ability of HAAM to promote central nerve growth [5].

The extracellular matrix (ECM) of HAMs did not change after acellular treatment of the amnion. The bioactive components maintaining HAAM mainly include collagen, fibronectin, laminin, and hyaluronic acid (HA). Among these

collagens are types I and IV to VI [6]. Collagen has hemostatic properties and is well-tolerated and bioabsorbable. The cellular activities of epithelial cells depend on the action of collagen [7]. Fibronectin is widely involved in tissue repair and cell migration. A considerable number of studies have used it to develop hemostatic materials [8]. HA is widely used in bioengineering to inhibit bacterial multiplication, promote mucosal recovery, and prevent scar growth. Many studies have used HA as a substrate to load bioactive materials [9]. Laminin bridges the differentiation and adhesive activities of different cell types [7, 8]. Furthermore, studies have shown that HAAM can promote angiogenesis and vascular remodeling by enriching angiogenic growth factors. Angiogenic growth factors, including basic fibroblast growth factor and vascular endothelial growth factor, are mainly derived from the basement membrane layer of HAAMs [10].

In response to the drawback of poor physical properties, many technical adjustments have been applied to HAAM [11]. First, HAAM is crushed, dissolved, and mixed with other biomaterials. In this process, the mechanical properties of HAAM are not significantly improved and the extracellular machinery of HAAM is destroyed. Some researchers have mixed HAAM with other cells or biomaterials to form a new ECM for axonal growth and regeneration [12]. However, in SCI, the injury site is relatively narrow, easily leading to peripheral blood supply obstruction, tissue edema, and scar formation. Ordinary HAAM mixed materials cannot achieve stable degradation or full filling, so the therapeutic effect of various bioactive factors of the amniotic membrane is limited. In summary, improving the mechanical properties of HAAM while maintaining its biological activity has become the primary problem that needs to be solved.

According to related studies, the chemical grafting of methacrylic anhydride (MA) to the ECM can fully retain its biological activity [13]. Moreover, combining biomaterials with hydrogels to enhance mechanical strength is a promising approach for SCI treatment [14]. Based on this concept, gelatin methacrylate (GelMA) is selected as the photocrosslinking carrier to ensure the release of its biological factors. At the same time, HAAM is chemically grafted with MA to form a two-component structure with GelMA instead of simple physical mixing (Fig. 1). In addition, the dialysis step in MA grafting can adequately eliminate the residual crosslinker. Rapid and stable photocrosslinking can prevent instability in the mechanical properties of the composite, thus avoiding the damage of the biological activity caused by the long treatment process. Therefore, GelMA–HAAMMA has great potential to be an ideal biocomposite scaffold for treating SCI.

This study evaluated the microscopic morphology, mechanical properties, and degradability of GelMA–HAAMMA. Furthermore, the ability of GelMA–HAAMMA was verified to coculture with neurons and increase the proliferative activity of human umbilical vein endothelial cells (HUVECs) in vitro. In the in vivo study, a spinal cord defect model in Sprague–Dawley (SD) rats was selected to verify the ability of GelMA–HAAMMA to promote nerve regeneration after SCI by pathological sectioning, immunofluorescence (IF) staining, and recovery of motor function at 4 weeks after surgery.

Materials and methods

Chemical reagents

MA was purchased from Shanghai Aladdin Biotechnology Company. Dulbecco's modified Eagle's medium (DMEM), neurobasal medium, and fetal bovine serum (FBS) were purchased from Thermo Fisher Scientific (China). GelMA was purchased from Suzhou EFL Biotechnology. Dialysis replacement membranes were purchased from Jerope Bio-Tech (USA). Primary antibodies against glial fibrillary acidic protein (GFAP) and Tuj-1 were purchased from Wuhan Sanying Life Technology (China). Secondary antibodies [goat anti-mouse IgG H&L (Alexa Fluor® 488), goat anti-rabbit IgG H&L (Alexa Fluor® 488), and goat anti-rabbit H&L (Alexa Fluor® 594)] were obtained from Shanghai Aladdin Biochemical Technology. Trypsin–EDTA (ethylene diamine tetraacetic acid, 0.25%) and penicillin–streptomycin were purchased from Wuhan Prosser Life Technology. Optimal cutting temperature (OCT) compounds were obtained from Beijing Sola Biotechnology. The hematoxylin-and-eosin (H&E) staining kit was purchased from Thermo Fisher Scientific. The Masson's trichrome staining kit was purchased from Solaibao Technology. The cell scraper and neuron extraction kit were purchased from Suzhou Solaibao Biotechnology. Matrigel was purchased from Preferred Biotechnology (Nanjing, China).

GelMA–HAAMMA synthesis

Decellularization of HAM

The HAMs used in this study were donated by the Department of Obstetrics, Affiliated Hospital of Nantong University. Fresh HAMs were washed thoroughly with phosphate-buffered saline (PBS) solution containing 0.1% (volume fraction) penicillin–streptomycin, cut into homogeneous sheets, and stored at −80 °C for 2 h. The mixture was taken out and melted at 37 °C. HAM was operated in three cycles of freezing and thawing. The samples were mixed with 0.25% trypsin–EDTA solution for 12 h at 4 °C and washed with DMEM at 4 °C, and epithelial cells were carefully scraped off with a cell scraper. The final product was weighed on a high-precision scale and dispensed in sterile Petri dishes

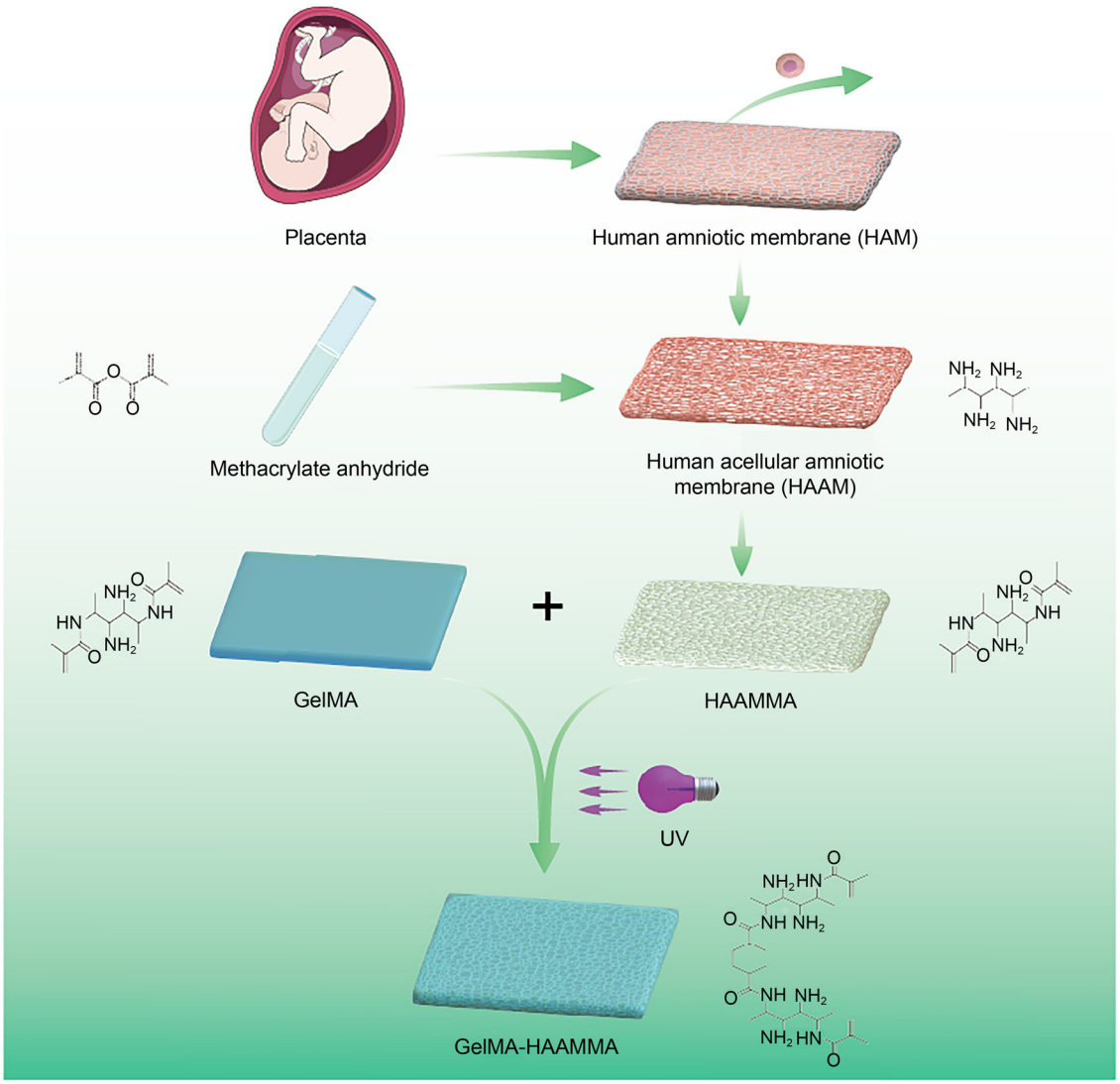

Fig. 1 Schematic preparation of GelMA–HAAMMA scaffolds for spinal cord injury repair . GelMA: gelatin methacrylate; HAAM: human acellular amniotic membrane; MA: methacrylic anhydride; UV: ultraviolet

containing ultrapure water. The weight of HAAM in each dish was approximately 1 g.

Identification of HAAM

The frozen sections were randomly selected from at least three sets of samples for staining. Each slice contained at least 1 cm^2 of HAAM. Following the standard H&E protocol, the successful decellularization of HAAM sections was verified under the microscope (Leica dm3000, Clinical Trial Center, Affiliated Hospital of Nantong University) after gradient dehydration with alcohol, washing with xylene, and sealing with neutral resin [10].

HAAMMA synthesis

PBS was used as a solvent to make the 4% (volume fraction) MA mixed solution, and HAAM was completely immersed in the solution and thoroughly stirred in a ventilated environment at 4 °C. The mixture was stirred every 2 h at 4 °C. Chemically grafted HAAMMA was obtained after 8 h. HAAMMA was washed repeatedly with PBS, loaded into dialysis bags (with a truncated molecular weight of 14–16 kDa), and dialyzed in ultrapure water for 36 h to remove unreacted MA. The samples were lyophilized and stored [15–17]. After weighing, each stored sample was 250 mg.

Chemical grafting modification of HAAM

The HAAMMA samples obtained in the previous step were dried in a drying box at 37 °C for approximately 30 min, then potassium bromide powder was added (mass ratio 1:100; Shanghai Aladdin Reagent), and the mixture was ground evenly [18]. The prepared product was put into a Fourier transform infrared spectrometer (FTIR) for analysis (Tianjin Jingtuo Instrument, China). The resolution of the instrument was set to 4 cm^{-1}, and the scan range used for the measurements was from 400 to 4000 cm^{-1} (number of scans 32, sampling gain 1.0, moving mirror speed 0.4747, detector DTGS KBr, and aperture 100.00).

GelMA–HAAMMA synthesis

Lyophilized GelMA (500 mg) was soaked in 10% (0.1 g/mL) PBS. GelMA in PBS was heated in a water bath at 70 °C for 30 min until completely dissolved. The solution was removed from the water bath and returned to 28 °C (room temperature, RT). Lyophilized HAAMMA (250 mg) was added to the above solution. Lithium phenyl(2,4,6-trimethylbenzoyl) phosphinate (0.001 g/mL) was added immediately after. In a biosafety cabinet, the mixed samples were continuously irradiated with an ultraviolet (UV) light emitting diode (LED) point light source (395–480 nm; Suzhou Yongqin Equipment, China) for 60 s to form a 2-mm-thick gel. The gel was dispensed with a sterile instrument at RT. One part of the gel was used to tamponade the SCI model, and the other was lyophilized at −80 °C for further verification [17].

Characterization and physical properties of GelMA–HAAMMA

Scanning electron microscopy (SEM) analysis

SEM was performed to observe the characterization of the mixed material. The mixed material was first cut into 1.2 cm × 1.2 cm films and fixed on the sample stage, and surface impurities were removed by washing with high-pressure nitrogen gas. The immobilization reagent was a conductive binder [19]. The surface of the sample was sprayed with gold (20 mA, 90 s) using a spray plating machine and observed under an S-5000 SEM (Guoyi Electronics, China).

Identification of the mechanical properties

The experimental groups were the HAAM, HAAMMA, GelMA, and GelMA–HAAMMA groups. At least three independent samples of 50 mm long and 12 mm wide were selected for each set of materials. The test temperature was 25 °C with the ambient humidity of 35%. First, the clamping distance of the machine was set to 30 mm. The sample was fixed with a clamped metal frame, and the head velocity was set to 10 mm/min. The test was started with an initial tensile force of 6 mN and a stepwise applied force gradient of 0.50 mN/min. The test was performed with a WSD series tensile testing machine (Wanchen, China) until the sample broke. Stress–strain curves were recorded for each sample, and their fracture strain values were calculated [17].

Degradation of GelMA–HAAMMA

Experimental grouping was consistent with groups described above. At least five random samples per group were selected to determine the degradation rate of GelMA–HAAMMA. The weight of each group of materials was not less than 250 mg. The mixed material was weighed to record the initial mass (W_0), which was embedded subcutaneously in SD rats with SCI, and the residual mass (W_1) was recorded at 0, 2, 4, 6, 8, 10, 14, 18, and 21 d. The material degradation rate was calculated as $[(W_0 - W_1)/W_0] \times 100\%$ [20, 21]. The experimental environment was the standard animal feeding environment in the Animal Experimental Center of Nantong University. The experimental animals were all mature SD rats with moderate body weight. Rats used for measurements were randomly selected experimental SD rats without skin-related diseases.

Swelling rate of GelMA–HAAMMA

To measure the swelling rate, five groups of GelMA–HAAMMA were prepared. The samples from each group were lyophilized, weighed (W_2), and put into a certain amount of PBS solution. The samples were removed at 2, 4, 6, 12, 24, and 36 h, and the surface was dried and weighed again (W_3). Each group of materials was returned to PBS at the end of each weighing, and swelling was calculated as $[(W_3 - W_2)/W_2] \times 100\%$ [22]. The final data were processed using GraphPad Prism version 8.0 (San Diego, CA, USA).

In vitro studies

Coculture of GelMA–HAAMMA and neurons

To verify the supportive and trophic effects of the composite hydrogel scaffold on neurons, neurons were extracted from neonatal 0–3 day old SD rats. The cell culture plates were coated with 20-fold diluted polylysine (10 mg/mL) for 3 h in a cell incubator at RT. The liquid was aspirated, and the plates were washed thrice with PBS. The cell slides were placed into each well plate for further planting. To verify the effect of coculture, GelMA–HAAMMA composite hydrogels were overlaid on a portion of the fixed cell slides. In another part of the well plates, only conditioned medium was added.

The implant solution was supplemented with DMEM/F-12 (42 mL), FBS (7 mL), 1% (volume fraction) penicillin–streptomycin, and L-glutamine (0.5 mL). The culture medium was supplemented with neurobasal medium (48 mL), B27 (1 mL), L-glutamine (0.5 mL), and 0.1% penicillin–streptomycin. The left and right cerebral hemispheres of neonatal SD rats were exposed, the superficial brain tissue was removed, and the crescent-shaped hippocampus was separated and placed in D-Hank's balanced salt solution. The blood vessels and meninges of the hippocampus were removed and placed into a centrifuge tube containing 4 mL implant fluid.

The mixture was mechanically blown 20–40 times and centrifuged for 5 min (1000 r/min). The supernatant was removed, 0.125% trypsin was added to the remaining liquid, and the mixture was blown 20 times and placed in a cell incubator at 37 °C for 5 min. The mixture was removed from the cell incubator, and trypsin digestion was terminated by adding DMEM. The mixture was filtered through a 200-mesh sieve and seeded in Petri dishes at a cell density of 1×10^8. The obtained cells were placed in a culture medium and cultured for 4–5 h, and the other cells that had adhered to the wall were discarded and centrifuged for 6 min (800 r/min). The supernatant was discarded, and the remaining cells were subsequently seeded in pretreated cell well plates with a culture medium. After the cells were fully adherent and grown, IF staining of neuron-specific antibodies was performed to verify the purification rate of neurons. Based on the periodicity of neurons cultured in vitro, the survival of neurons for three days was tested to avoid the influence of culture medium toxicity on the experimental results [23]. At least five cell slides from the two sets of well plates were selected for trypan blue staining on Days 1 and 3 of coculture. The stained cells were observed and measured with a cell counter (Rayward, Shenzhen, China).

Tube formation and cell migration assays

HUVECs were donated by the Department of Obstetrics, Affiliated Hospital of Nantong University. HUVECs were cultured in an endothelial cell culture medium (5% FBS and 1% penicillin–streptomycin) at 37 °C with 5% CO_2.

For cell migration assays, HUVECs were seeded in 6-well plates (1.5×10^5 cells/well) and cultured until 100% confluence. The experimental groups were the control, GelMA, and GelMA–HAAMMA groups. Five parallel scratch holes were made in each well with a 100 μL pipette tip, and 1 mL medium was added to each well, some of which contained a GelMA–HAAMMA composite scaffold (50 mg; $n = 6$). One of the remaining 6-well plates was supplemented with only 100 μL medium as a control, and the other was supplemented with GelMA (50 mg) and 100 μL medium. Migration rates were observed under a light microscope after 24 h and measured immediately using ImageJ [10].

For angiogenesis experiments, 50 μL Matrigel was added to each well of a 96-well plate, and gel formation occurred at 37 °C. HUVECs were starved for 24 h and added to 96-well plates (cell density 2×10^4), 100 μL medium was added to each well, and GelMA–HAAMMA was simultaneously added to each well of the plates ($n = 3$) [24]. The grouping of this experiment was consistent with cell migration assays. After 6 h, angiogenesis was observed using an inverted light microscope (Olympus, Japan).

In vivo studies

The experimental animals in this study were all female SD rats (eight weeks old, weighing 250 g). The animals were fed in an animal laboratory environment at 25 °C. The animal laboratory was equipped with a 12 h light–dark cycle (from 8 a.m. to 8 p.m.).

In the SCI simulation, a laminectomy of the T10 segment was chosen. Before surgery, female SD rats were anesthetized via an intraperitoneal injection of 25 mg/kg anesthetics (sodium pentobarbital). The spinal cord was dissected evenly from the middle to the left side using a designed surgical scalpel, separated by 2 mm, resulting in defects in the left hemisphere of the rat spinal cord. SD rats were randomly divided into four groups with 15 rats in each group: a sham operation group with laminectomy only (sham group), an SCI group, a GelMA group implanted with GelMA hydrogel, and a GelMA–HAAMMA group implanted with GelMA–HAAMMA composite hydrogel scaffold. Experimental SD rats were carefully sutured to the muscle, fascia, and epidermis, and incisions were sterilized with iodine. To prevent infection and reduce pain, rodents were injected with buprenorphine and penicillin. After surgery, the rats were assisted in manually expelling urine from the bladder (thrice daily) until urination returned to normal. At the 4 weeks postoperatively, SD rats were euthanized, and spinal cord tissue was obtained by dissection [25].

Postoperative functional recovery

To observe the functional recovery after SCI, the Basso, Beattie and Bresnahan (BBB) score was selected as the evaluation standard. The BBB score is a rating scale ranging from 0 to 21. At 0, 1, 3, 7, 14, 21, and 28 d after SCI, SD rats with SCI were allowed to roam freely in a closed environment for statistical observation. The personnel observing and scoring were unaware of the SD rat grouping. Each group of SD rats was handled by three randomly assigned team members. The three members counted separately and did not communicate with each other about the results.

Histology of the spinal cord

At 4 weeks after SCI, SD rats were euthanized, and hearts were perfused with normal saline (200 mL), followed by fixation with 4% paraformaldehyde. The members of the spinal cord containing the lesion site were removed by dissection, fixed with 4% paraformaldehyde for 24 h, and immersed in sucrose solution at different concentrations for dehydration. The spinal cord was encased in OCT. Tissues were processed in a cryomicrotome (lica-cm1950, Clinical Experimental Center, Affiliated Hospital of Nantong University) to obtain 8–12 μm thick coronal sections.

H&E and Masson staining

According to the standard protocol of Masson staining preparation and H&E staining, frozen sections from each experimental group were randomly selected for staining. After dehydration and fixation, the prepared sections were photographed with a light microscope (Leica dm3000) and analyzed with ImageJ (National Institutes of Health).

IF staining of spinal cord sections

Frozen sections were thawed for 35 min at RT and washed with PBS. The sections were incubated with 0.3% Triton X-100 containing 10% goat serum for 60 min at RT. The primary antibody was subsequently added to the slides and incubated at 4 °C for 16 h before adding the secondary antibody. After incubation for 2 h at RT, the sections were washed thrice with PBS, and the nuclei were stained with 4′,6-diamidino-2-phenylindole (DAPI). All sections were observed under a Keyence fluorescence microscope and photographed.

Statistical analysis

Statistical analyses were conducted using GraphPad Prism version 8.0 (San Diego, CA, USA). For sample size calculation, the statistical power was set at 0.90, and the significance level was set at 0.05. The corresponding minimum sample size was calculated based on the effect size of the different experiments. The data of each group were calculated as mean ± standard deviation (SD). Statistical differences between groups were compared using analysis of variance (ANOVA). Two-way repeated measures ANOVA was used to analyze BBB scores. The SNK-q test was used to compare the means of data from multiple groups. $p < 0.05$ indicated statistical significance; at least three trials were performed for each experiment.

Results

HAAM and HAAMMA preparation

In Fig. 2a (top), freshly obtained HAM is a pink film, consistent with its nature as the thickest basement membrane in the human body. After the decellularization steps described above, in Fig. 2a (bottom), the successfully decellularized HAMs became transparent, significantly reduced in weight, and could float in the stored ultrapure water. Figure 2b shows the H&E staining verification performed to verify HAM decellularization. As shown above, nuclei labeled with hematoxylin can be seen in the stained image of normal HAMs. The nuclei were neatly arranged in the epithelial layer of HAMs. In the bottom, however, the number of nuclei in the staining result is 0 ($n = 5$). Therefore, based on the double verification of gross observation and staining images, HAM was successfully decellularized into HAAM. This confirmed the successful preparation of HAAM [10].

Figure 2c shows the scanning electron microscope (SEM) verification of HAM and chemically grafted HAM. The top part shows the cell-free structure and fibrous connections of HAAM. The bottom part shows the structure and fibrous connections of HAAMMA. By comparison, the backbone structure and fiber connections in HAAMMA were not changed or even destroyed after chemical grafting. Figure 2d shows the results of infrared (IR) spectra to judge whether the grafting of MA is effective. The top part shows the distribution of the characteristic peak of the IR spectra of HAAM. The amide A band of normal HAAM was concentrated at 3290 cm^{-1}. The peak value was mainly determined by the N–H vibration contraction. The bottom part shows no significant destruction or change in the backbone structure of HAAMMA, whose characteristic peak of acrylamide appeared at 3396 cm^{-1} [15, 17], indicating that the grafting of MA was successful.

Representation of GelMA–HAAMMA

Due to the dense network structure of traditional biomaterial scaffolds, it is difficult for newborn cells to freely pass through them. Figures 3a and 3b show the SEM results of HAAM and HAAMMA, respectively, which showed a porous fibrous network structure. This confirms the inherent defect of HAM as a film-like biomaterial. In treating spinal cord defects, HAM has a good restorative effect because of its rich ECM and various nutritional molecules. However, it is difficult for newborn neurons to reach the contralateral side through the original HAM. Acellular treatment or chemical modification did not change the HAM structure. Only by turning HAM into a three-dimensional (3D) ordered structure can the performance of biomaterials be maximized. Figure 3c shows the 3D structure electron micrographs of GelMA. The

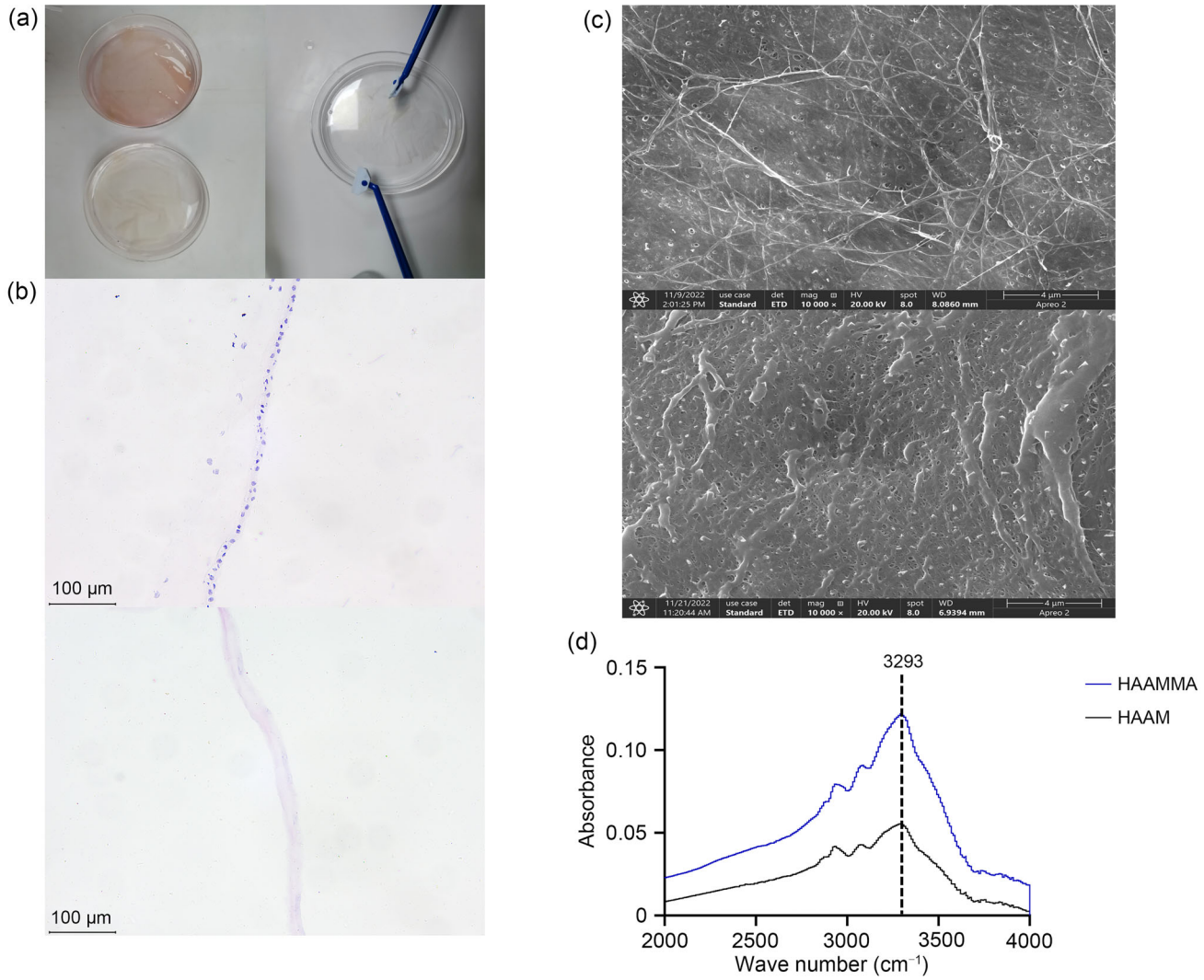

Fig. 2 Preparation of HAAM and HAAMMA. **a** Decellularization of HAM. **b** H&E staining of human amniotic membrane after decellularization. Scale bar: 100 μm (×10). **c** SEM images of HAAM and HAAMMA. Scale bar: 4 μm (×10,000). **d** Differences in IR spectra between HAAM and HAAMMA indicate the presence of grafting and the formation of new bonds. HAAM: human acellular amniotic membrane; MA: methacrylic anhydride; HAM: human amniotic membrane; H&E: hematoxylin-and-eosin; SEM: scanning electron microscopy; IR: infrared

pore size distribution was relatively uniform, and the structure was stable, with an average pore size of (53 ± 10) μm (Fig. 3e). In Fig. 3d, the structure of GelMA–HAAMMA was similar to that of GelMA. However, the pores of GelMA–HAAMMA were more uniform, and most of them were elliptical, with an average pore size of (26 ± 9) μm (Fig. 3f). There was a very significant difference in pore size between GelMA and GelMA–HAAMMA ($p < 0.05$). Considering the characteristics of newborn and peripheral blood-derived cells in the spinal cord defect, GelMA–HAAMMA is more suitable for guiding SCI recovery and regeneration.

Figure 4a shows the maximum load values of the four groups of materials after the mechanical tensile test. The HAAM, HAAMMA, GelMA, and GelMA–HAAMMA results were (0.47 ± 0.01), (2.51 ± 0.03), (3.35 ± 0.05), and (4.18 ± 0.06) MPa, respectively. SCI usually affects the movement of the corresponding segment of the limb. The injured site still has some degree of activity during the recovery period. To achieve continuous and stable degradation of composite scaffolds in the spinal cord after injury, it is necessary to have an excellent elastic modulus as a support [17]. The elastic modulus of HAAM, HAAMMA, GelMA, and GelMA–HAAMMA were (1.78 ± 0.07), (6.16 ± 0.12), (14.29 ± 0.24), and (19.69 ± 0.52) MPa, respectively (Fig. 4b). GelMA–HAAMMA had the best elastic modulus ($p < 0.05$), ensuring that it does not deform with

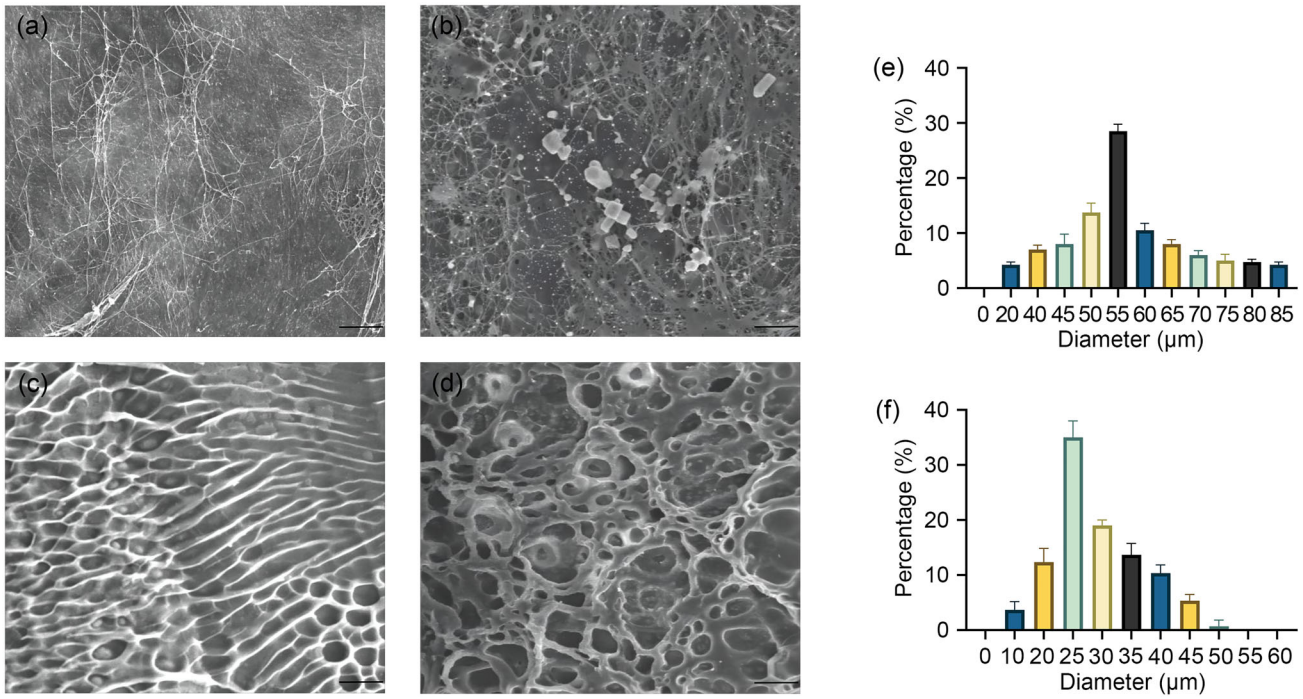

Fig. 3 SEM images and pore size frequency distribution. **a**–**d** SEM images of HAAM, HAAMMA, GelMA, and GelMA–HAAMMA, respectively. Scale bar: 20 μm. **e**, **f** Plots of diameter frequency distribution data for GelMA and GelMA–HAAMMA, respectively. Data are expressed as mean±standard deviation ($n = 3$). GelMA: gelatin methacrylate; SEM: scanning electron microscopy; HAAM: human acellular amniotic membrane; MA: methacrylic anhydride

body movement in the damaged area. In this way, the area through which the newly formed axons pass in the scaffold can be stabilized for a long time after injury [26]. Statistical results showed that the mechanical properties of the GelMA–HAAMMA group were significantly stronger than those of the other groups ($p < 0.05$). The composite inherits the mechanical properties of GelMA and is superior to pure hydrogel.

Figure 4c shows the degradation rates of the four groups of materials. The degradation rate of HAAM was the highest, nearly completely degraded on Day 10. HAAMMA was 100% degraded on Day 11. There was no significant difference between the two groups ($p > 0.05$). Inheriting the degradation ability of GelMA, GelMA–HAAMMA is completely degraded on Day 15. There was no significant difference in degradation ability between GelMA and GelMA–HAAMMA ($p > 0.05$), but both were better than HAAM and HAAMMA ($p < 0.05$). Further studies by our team could concentrate on optimizing the degradation rate.

The water absorption capacity of the four groups of materials was measured. On the one hand, the biomaterial can quickly absorb water and expand, which can effectively plug and stop bleeding in the SCI area. On the other hand, the biomaterials absorb nutrients from the body by absorbing water, and provide a good microenvironment for cell proliferation and nerve regeneration. The swelling rate reflects the aiding effect of the biomaterials on the rapid healing of the injury. Figure 4d summarizes the swelling rates of the four groups of materials. Unfortunately, HAM and HAAMMA have poor absorptive capacity. HAM and HAAMMA were counted again separately (Fig. 4e). The swelling rate of GelMA–HAAMMA reached its highest peak of $(407 \pm 3)\%$ ($n = 5$) on Day 24, the swelling rate of GelMA reached its highest peak of $(497 \pm 5)\%$ ($n = 5$) on Day 28, and the swelling rates of HAAM and HAAMMA peaked at 24 d, which were both $(6.96 \pm 0.14)\%$ ($n = 5$). The reason for the inferior results of GelMA–HAAMMA compared to the GelMA group is the deficiency of absorption capacity of HAM itself [17, 27].

In vitro cellular experiments

In the cellular experiment, the first thing to determine is whether the composite hydrogel supports neuronal growth, which is crucial for its application in SCI. The difficulty of extracting neurons is that the culture medium must be changed at the precise time point after cells are seeded in the culture flask, and cells must be centrifuged quickly. The differential adherent separation technique was used to distinguish neurons from other cells. Therefore, it is particularly

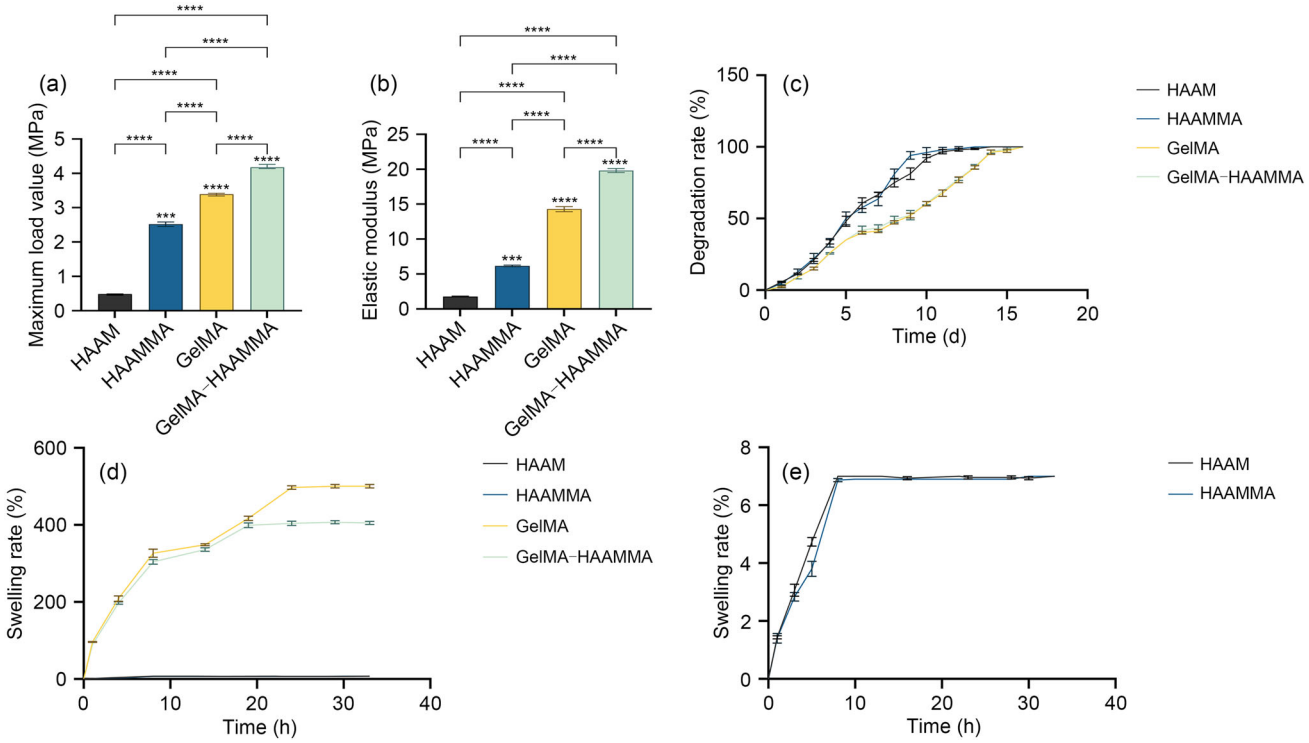

Fig. 4 Characterization of composite hydrogels. **a** Maximum load values for HAAM, HAAMMA, GelMA, and GelMA–HAAMMA. **b** Elastic modulus of HAAM, HAAMMA, GelMA, and GelMA–HAAMMA. **c** Degradation rates of HAAM, HAAMMA, GelMA, and GelMA–HAAMMA. **d** Swelling rates of HAAM, HAAMMA, GelMA, and GelMA–HAAMMA. **e** Expansion of swelling rates of HAAM and HAAMMA. Data are expressed as mean ± standard deviation ($n = 5$). $^{***}p < 0.001$; $^{****}p < 0.0001$. HAAM: human acellular amniotic membrane; MA: methacrylic anhydride; GelMA: gelatin methacrylate

important to verify the proportion of neurons in the extracted cells. Figure 5a shows the growth of extracted neurons in the conditioned medium, and Fig. 5b represents the distribution of neuronal growth under GelMA–HAAMMA coculture conditions. Nuclei located by DAPI staining are shown in blue, and expression of neuron-specific antibodies is shown in green. Localization of nuclei in the merged images coincided with neuronal antibody staining. IF results confirmed that the extracted cells were clearly neurons. Under the fluorescence microscopy, the characteristic morphology of neurons in the two groups of different culture environments could be clearly observed, including cell bodies, dendrites, and axons. More than 90% of the cells in both groups were neurons as calculated by ImageJ ($n = 10$; Fig. 5e). According to the instructions of the cell viability staining reagent, trypan blue staining is the most convenient for statistics when the purification rate of cells is >90%. Therefore, the more convenient method of trypan blue staining was chosen to calculate cell survival.

At the SCI site, neurons take up less than the total amount of nutrients available under normal body conditions. GelMA–HAAMMA can continuously provide various trophic factors for nerve regeneration after application at the injured site. After verifying the proportion of neurons, a low concentration of medium (0.5 g/mL) was added to the control and GelMA–HAAMMA groups one day later to simulate the nutritional environment of the body after injury. Figure 5c shows trypan blue cell survival images at 1 and 3 d of the control group, and Fig. 5d shows the results of the GelMA–HAAMMA group. Green cells in the image represent survival by color flipping of the counter. On the third day, the survival rate of the neurons in the GelMA–HAAMMA group was notably greater than that in the control group. After three days, the number of surviving neurons in the GelMA–HAAMMA group was not statistically different from before ($p > 0.05$; $n = 5$). At the same time, the survival rate of neurons in the control group was significantly reduced by (7 ± 1.1)% ($p < 0.05$; $n = 5$; Fig. 5f). Cell survival analysis revealed that the GelMA–HAAMMA scaffold could maintain neuronal activity and had good biocompatibility with neurons. The HAAM active components in the composite hydrogel provide nutrients for neuronal growth.

In the SCI recovery process, the rapid reconstruction of new blood vessels at the defect is also significant. Neovascularization involves nutrient transport, immune regulation,

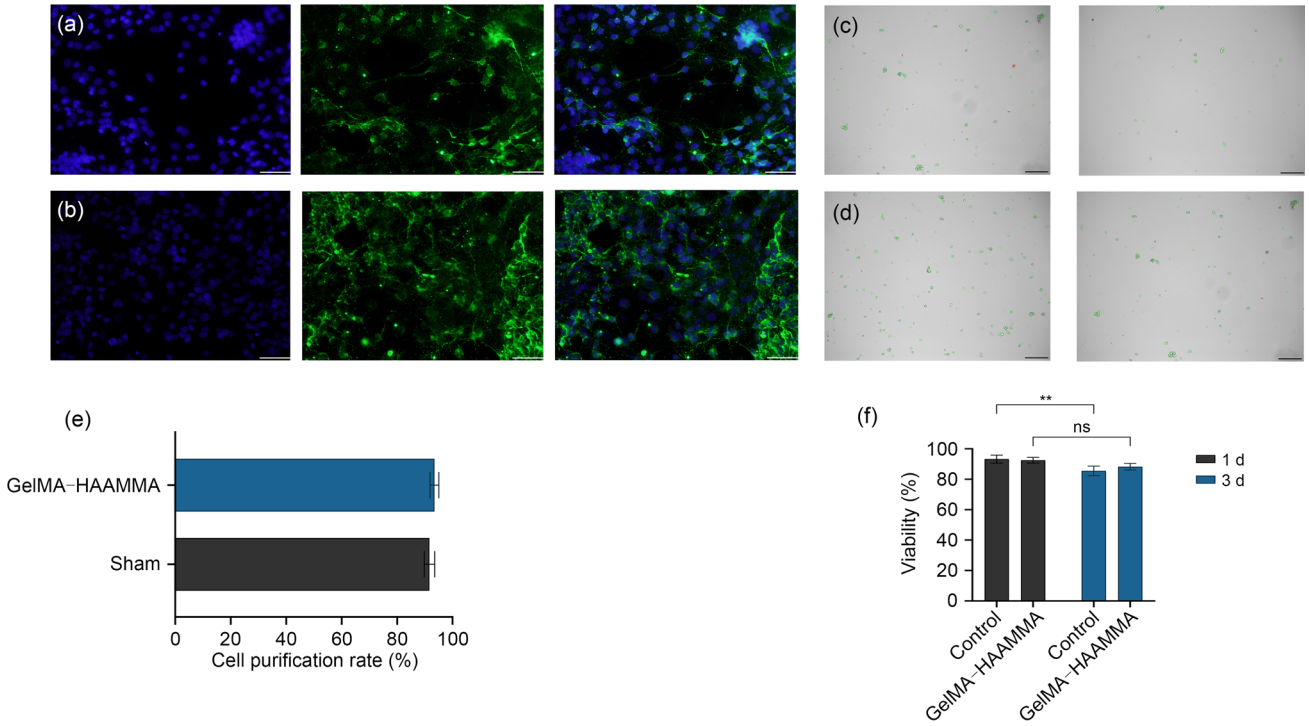

Fig. 5 Coculture of neurons and GelMA–HAAMMA. **a** Normal neurons. Scale bar: 200 μm (×10). **b** Neurons cocultured with GelMA–HAAMMA. Scale bar: 200 μm (×10). **c** Survival of normal neurons after 3 days. Scale bar: 5 μm (×100). **d** Survival of cocultured neurons after 3 days. Scale bar: 5 μm (×100). **e** Statistics of neuronal purification rates. **f** Statistics of neuronal 3-day survival experiments. Data are expressed as mean±standard deviation ($n = 5$). $^{**}P<0.01$; ns: not significant. GelMA: gelatin methacrylate; HAAM: human acellular amniotic membrane; MA: methacrylic anhydride

and scar formation [28, 29]. First, the effect of the composite hydrogel on HUVEC proliferation was tested. Figure 6a shows the microscopic images of scratch experiments of cells in different groups. As shown in Fig. 6b, the migration rate of the GelMA–HAAMMA group was 0.4237±0.078 higher than that of the control group, and was 0.2339±0.09 higher than that of the GelMA group (n=6). Cell migration assay results revealed that the ability of the GelMA–HAAMMA group to promote HUVEC proliferation was significantly greater than that of the other groups. To further investigate the proangiogenic ability of the composite hydrogel, Fig. 6c shows the microscopic results of the in vitro angiogenesis assay. The GelMA–HAAMMA group produced more neovascularization than the other two groups. As shown in Fig. 6d, the number of tubes per field of the GelMA–HAAMMA group was 111±10.59 higher than that of the control group, and was 57.89±9.307 higher than that of the GelMA group ($n = 6$) [10, 30]. The composite hydrogel effectively inherited the proangiogenic biological activity of HAAM, which is of great help for the reconstruction of neovascularization after SCI.

Recovery from SCI in vivo

Inhibiting collagen scar formation and maintaining the stability of new tissue

After SCI, glial scar formation at the injury site will hinder nerve regeneration and repair. With the extension of time, scar contracture will lead to further expansion of the defect site and even syringomyelia. Previous studies have shown that the 3D structure of hydrogels can alleviate this problem without causing severe spinal cord defects. However, this can only inhibit the expansion of the injury rather than promote nerve repair [26, 31]. H&E staining was used to observe tissue homeostasis (Fig. 7). H&E staining results are usually used to observe the overall tissue morphology and local recovery. Because statistical significance is usually modest, the results in the figures are only for tissue homeostasis assessments. The GelMA–HAAMMA group had the least scar production and the most solid tissue recovery compared to other groups. After the overall evaluation, Masson staining was used to quantify the area of the collagen scar and verify the efficacy of the composite hydrogel. In Fig. 8a, the GelMA–HAAMMA group had significantly fewer areas of collagen staining than that in the other groups. In Fig. 8b, the proportion of blue

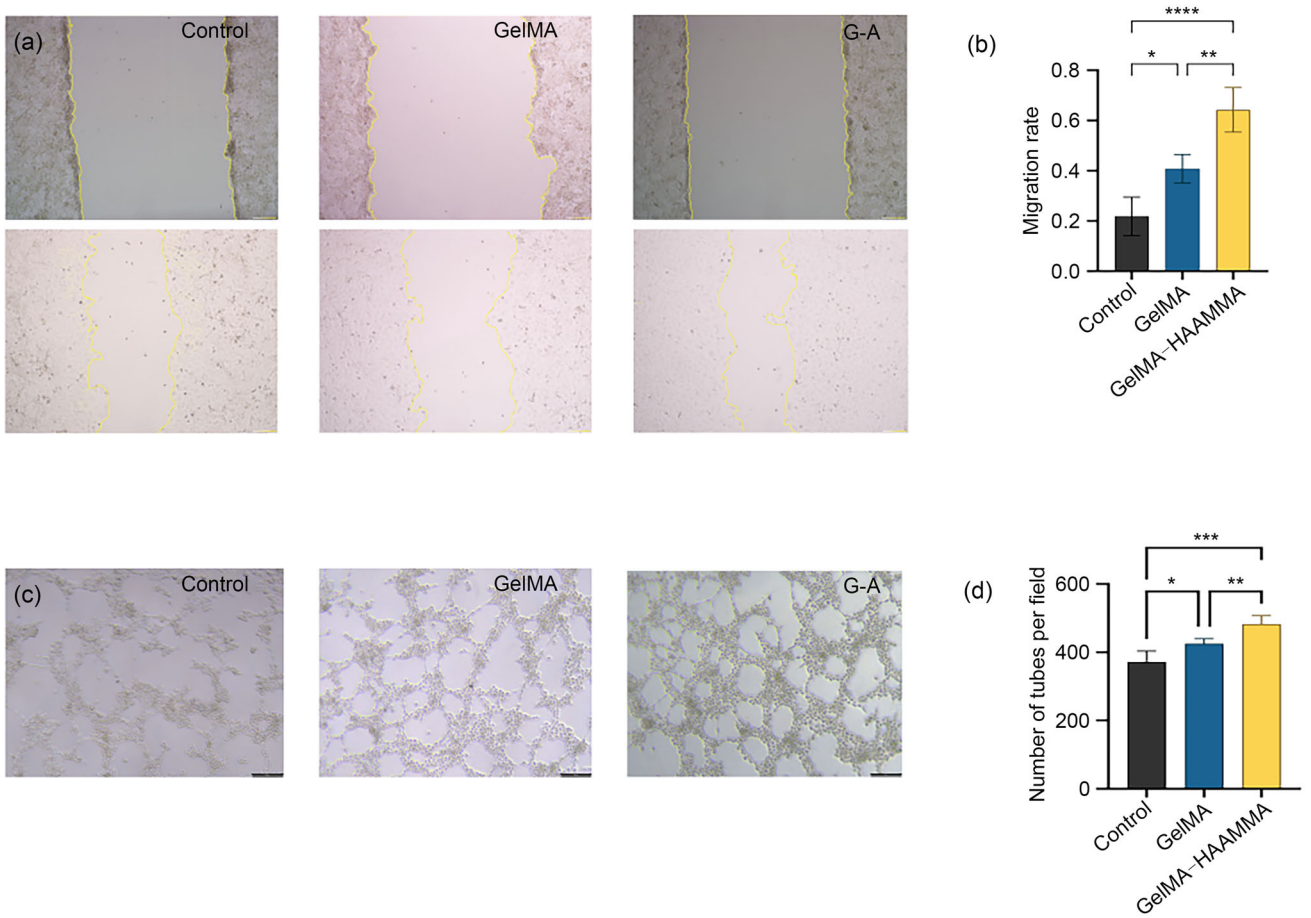

Fig. 6 The effect of GelMA–HAAMMA on HUVECs in vitro. **a** Cell migration at 24 h. Scale bar: 200 μm (×5). **b** Statistics of cell migration ($n = 6$). **c** Tube formation after 6 h. Scale bar: 200 μm (×5). **d** Statistics of tube formation data. Data are expressed as mean ± standard deviation ($n = 3$). $^{*}p < 0.05$; $^{**}p < 0.01$; $^{***}p < 0.001$; $^{****}p < 0.0001$. GelMA: gelatin methacrylate; HAAM: human acellular amniotic membrane; MA: methacrylic anhydride; HUVECs: human umbilical vein endothelial cells; G-A: GelMA–HAAMMA

area in the SCI group was (35.37 ± 0.7)% higher than that in the sham group. The proportion of blue area in the GelMA group was (9.63 ± 0.7)% higher than that in the sham group. The proportion of blue area was (2.5 ± 0.65)% higher in the GelMA–HAAMMA group (G-A in the figure) than that in the sham group ($n = 3$). The above results showed that GelMA–HAAMMA had excellent anti-glial scar formation ability as a composite hydrogel.

Improvement in motor function after SCI

The nerve regeneration result after SCI is the gradual recovery of the body's motor function. The BBB score is a reliable index for evaluating the recovery of motor function after SCI in SD rats. In Fig. 9d, the left hindlimb of each SD rat showed normal motor function before surgery (score = 21). After a defect in the left spinal cord, rats developed complete paralysis of the left hindlimb. The scores of the SCI and GelMA groups did not reach 7 at two weeks after the operation, which showed that the self-repair ability of rats after SCI was limited. In the GelMA–HAAMMA group, the recovery of motor function in the SD rat group was clearly greater than that in the other groups at two weeks after surgery. At four weeks after surgery, GelMA–HAAMMA rats performed sustained palm-bearing movements and coordinated hindlimb movements with a score of 15–16. These results proved that GelMA–HAAMMA promotes motor function recovery [32, 33].

Regeneration of neurons and axons

To further investigate the effects of GelMA–HAAMMA (G-A in the figure) on nerve regeneration, IF staining on the spinal cord sections of rats was performed at four weeks after surgery. The same observation method was followed for IF as did for section staining. The whole tissue was first

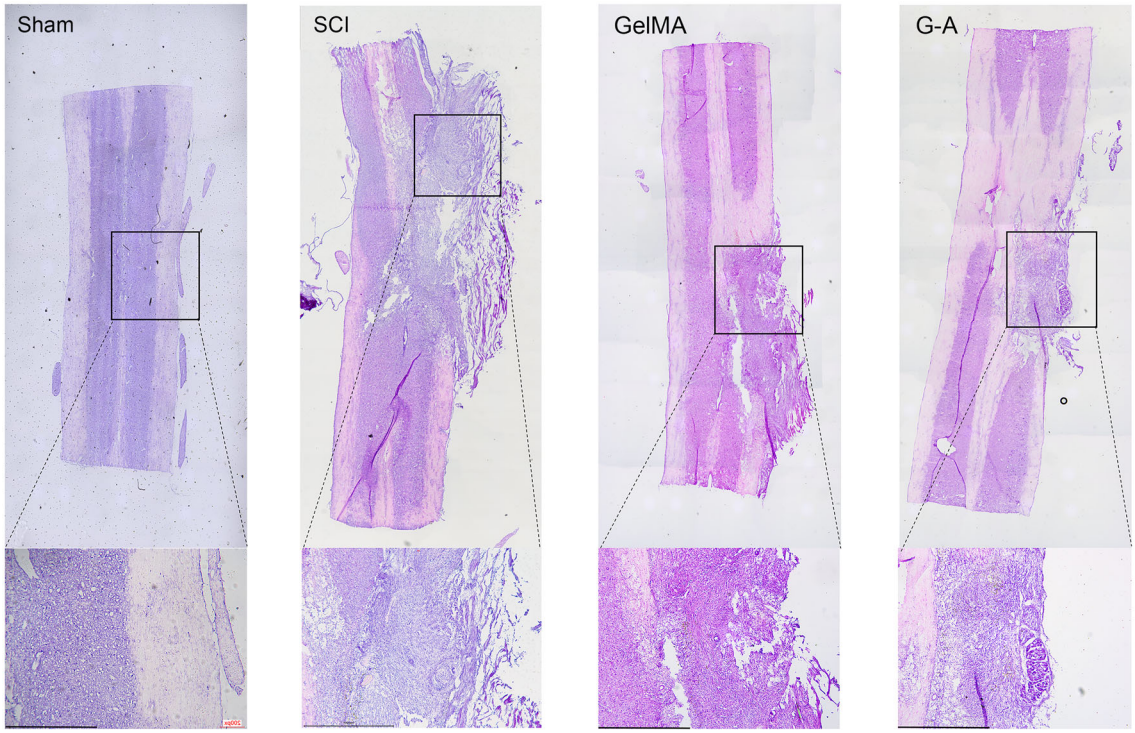

Fig. 7 Histological analysis of the four groups four weeks after operation. Representative images of H&E staining. Scale bar: 200 μm (× 10). H&E: hematoxylin-and-eosin; SCI: spinal cord injury; GelMA: gelatin methacrylate; HAAM: human acellular amniotic membrane; MA: methacrylic anhydride; G-A: GelMA–HAAMMA

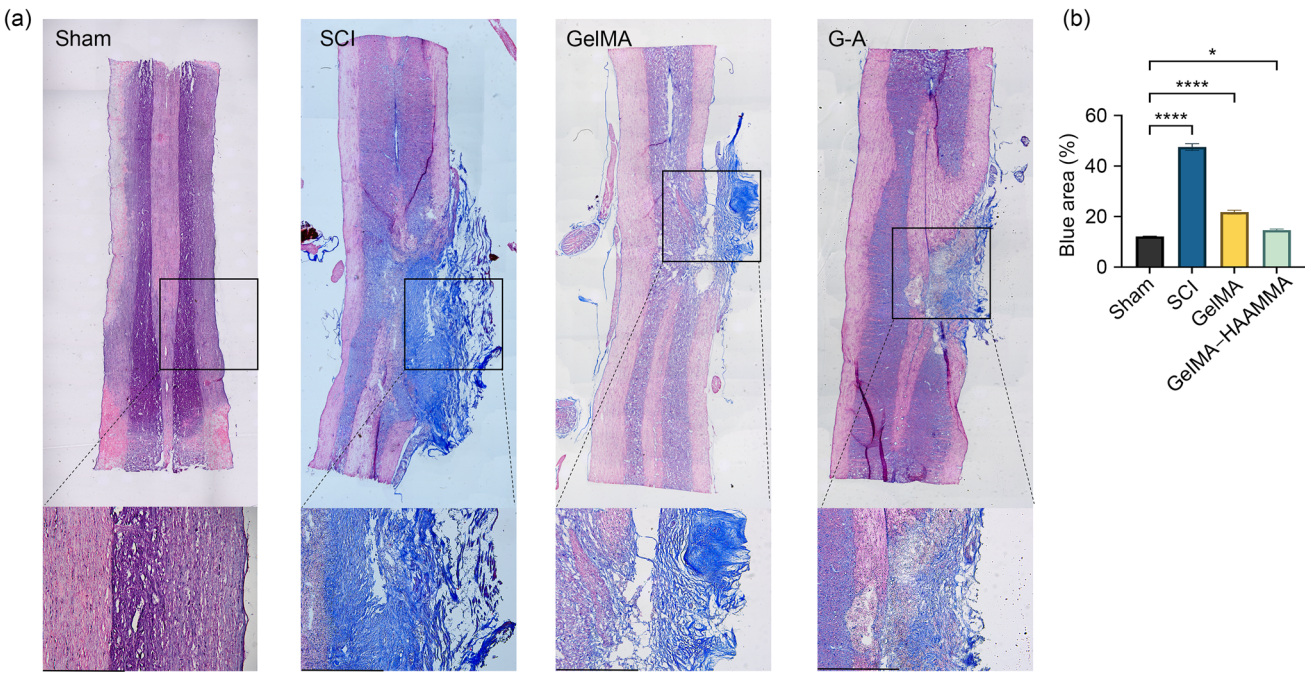

Fig. 8 Inhibition of scarring in spinal cord tissue by GelMA–HAAMMA at 4 weeks after surgery. **a** In the representative images of Masson's trichrome staining, collagen tissue is stained blue. Scale bar: 200 μm (×10). **b** Statistics of blue areas stained with collagen. Data are expressed as mean±standard deviation (n=3). $^{*}P<0.05$; $^{****}P<0.0001$. GelMA: gelatin methacrylate; HAAM: human acellular amniotic membrane; MA:methacrylic anhydride; SCI: spinal cord injury; G-A: GelMA–HAAMMA

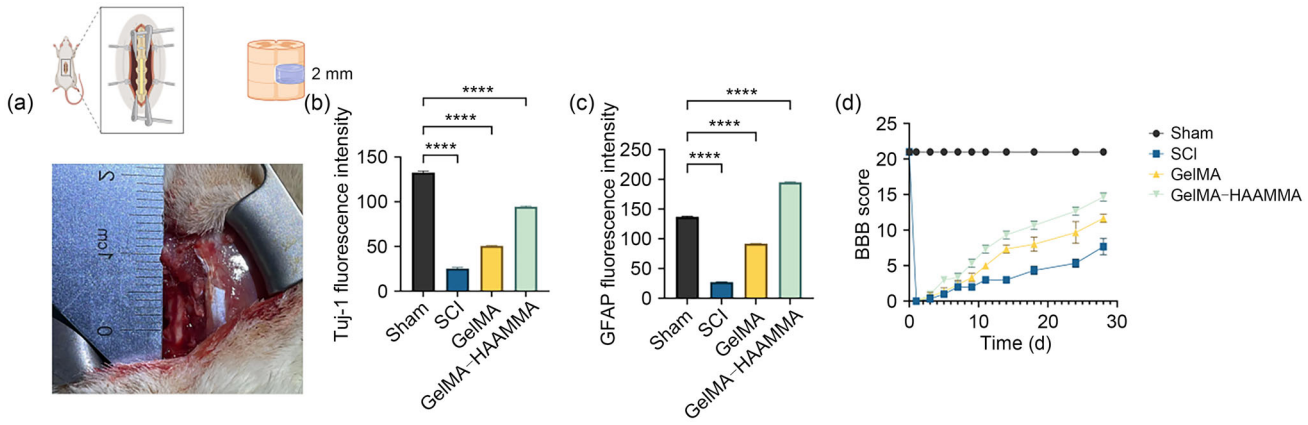

Fig. 9 Effects of GelMA–HAAMMA on neuronal growth and recovery of motor function. **a** Schematic diagram of the rat's left spinal cord hemisection injury model. **b** Graph of the Tuj-1 IF intensity quantification. **c** Graph of the GFAP IF intensity quantification. **d** Left hindlimb locomotor recovery was measured by the BBB scale. Rats treated with GelMA–HAAMMA had improved BBB locomotor scores. All data were statistically analyzed by two-way ANOVA ($n = 5$). Data are expressed as mean ± standard deviation ($n = 3$). $^{****}p < 0.0001$. GelMA: gelatin methacrylate; HAAM: human acellular amniotic membrane; MA: methacrylic anhydride; IF: immunofluorescence; GFAP: glial fibrillary acidic protein; BBB: Basso, Beattie and Bresnahan; ANOVA: analysis of variance; SCI: spinal cord injury

observed under the microscope, and the injury site was magnified for statistics. Figure 10 shows the overall morphology of the sectioned tissues in different groups under IF. The blue area is the nucleus after DAPI staining. Green fluorescence is a marker of high expression of neuronal antibodies. In red, astrocytes are labeled with GFAP antibodies. By DAPI staining, the SCI group had much more hypertrophic scar tissue than other groups. The histological morphology of GelMA and GelMA–HAAMMA groups was similar to the results of Masson staining. The recovery of the injured area was analyzed. In Fig. 10, many Tuj-1-positive neurons were detected in the G-A group, whereas the percentage of Tuj-1-positive neurons was lower in the SCI and GelMA groups.

Figure 9a shows the schematic design of the animal experiment and the actual filming during the operation. Based on statistical analysis (Fig. 9b), the neuronal fluorescence intensity in the SCI group was 107.4 ± 1.07 lower than that in the sham group. The fluorescence intensity of neurons in the GelMA group was 82.04 ± 1.074 lower than that in the sham group. The fluorescence intensity of neurons in the GelMA–HAAMMA group was 38.15 ± 1.0 lower than in the sham group. Compared to other groups, the effect of the GelMA–HAAMMA group on promoting nerve regeneration was very obvious, and the difference between the number of neurons in the normal spinal cord was minimal. Based on the above results, GelMA–HAAMMA effectively promoted neuronal regeneration [12, 34]. Moreover, collagen abundance in HAAM greatly increased the percentage of GFAP-positive cells (Fig. 9c). The fluorescence intensity of GFAP in the GelMA–HAAMMA group was even higher than that in the sham group by 58.10 ± 0.58. Whether there was any other correlation between this phenomenon and HAAM remains to be further explored.

Discussion

Despite its excellent tissue regeneration potential, HAAM is limited by its thin physical shape and poor mechanical properties. It is difficult to avoid folding or tearing when dealing with thin sheets of HAAM [35]. Previous studies have shown that composite biomaterials can compensate for the defects of biomaterials by combining the active factors of biomaterials with the good mechanical properties of scaffolds [28]. In this study, HAAM and GelMA hydrogels were synthesized as novel photocrosslinked materials with a double-layer network crossover structure. The composite had the physical and chemical properties of gelatin and inherited the biological activity of HAAM itself. In SCI, composites can mimic the ECM microenvironment effectively, regulate pathological processes, and promote neuronal regeneration. The comprehensive ability of composite materials comes from their physical properties and biological components.

GelMA is rich in hydrophilic polymers and forms a porous composite structure that can absorb a large amount of water in tissues and provide a good nutritional environment for cell growth and development [36]. HAAM is rich in collagen, in which the amino group reacts with MA, and the methacryloyl group is transferred to form HAAMMA. FTIR spectroscopy results also showed that such chemical grafting was successful. The backbone structure of HAAM was not destroyed. Only when the main structure of HAAM is preserved can its biological activity be fully displayed in the SCI recovery.

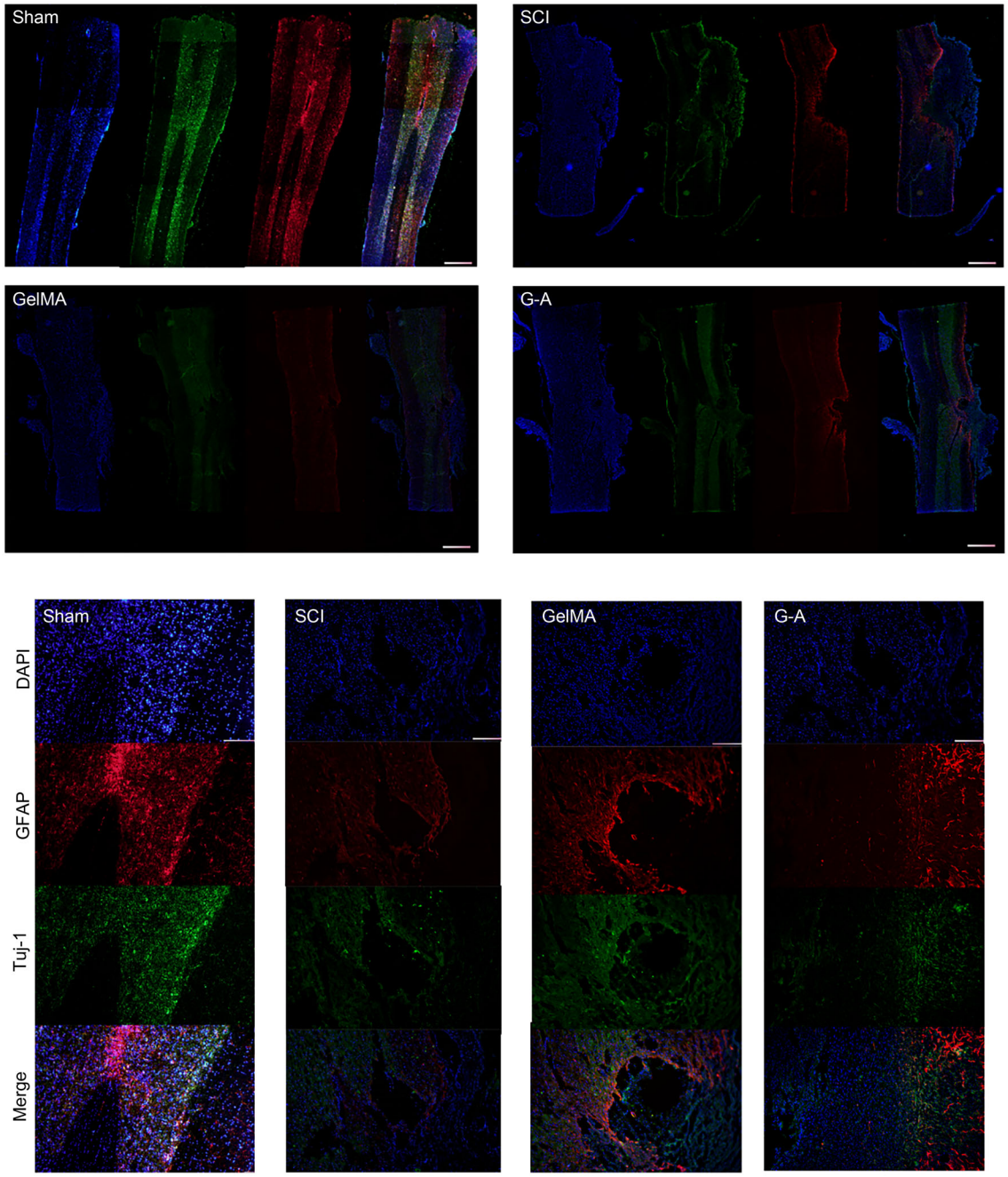

Fig. 10 Overall immunofluorescence images of treatment effects after spinal cord injury in the four groups. Scale bar: 500 μm (×4). Locally enlarged images: promoting effect of GelMA–HAAMMA (G-A) on nerve regeneration after spinal cord injury. Tuj-1 (green) neurons, GFAP (red) astrocytes, and nuclei stained with DAPI (blue). Scale bar: 100 μm (× 10). GelMA: gelatin methacrylate; HAAM: human acellular amniotic membrane; MA: methacrylic anhydride; SCI: spinal cord injury; DAPI: 4′,6-diamidino-2-phenylindole; GFAP: glial fibrillary acidic protein

Successful chemical grafting is the key to photocrosslinking of composite hydrogels.

Referring to Zhang's method [17, 19], this study used lithium phenyl phosphinate as a photoinitiator, which can complete the photocrosslinking process in a short time, to avoid long-term UV damage to DNA and cell function. After photocrosslinking, the composite scaffolds exhibited a bilayer interpenetrating structure, and the mechanical properties of HAAM were significantly enhanced.

Tissue engineering scaffolds for SCI must have sufficient biomechanical properties to support the passage of

nerve axons. Excellent mechanical strength is an important prerequisite for composite hydrogels to firmly fill spinal cord defects and provide ECM environment [37]. With stable degradation of the composite scaffold, the newborn neurons could stably survive in the injured area. Through previous experiments, the mechanical properties of GelMA–HAAMMA formed after photocrosslinking were obviously greater than those of HAAM and GelMA. The degree of chemical crosslinking of GelMA–HAAMMA was greater than that of GelMA, so water absorption was reduced, preventing significant swelling in the spinal cord defect. SCI is often accompanied by massive bleeding. If the expansion rate of implanted biomaterials increases significantly after water absorption, the damaged area will be severely expanded. The recovery time of the broken end of the central nervous system will be greatly extended due to the expansion of the damaged area [38]. The swelling rate of the composite was further decreased compared to that of GelMA, proving that it does not affect the damaged area after in vivo implantation. At the same time, the deformation degree of the composite scaffold was better than that of the ordinary GelMA scaffold. As mentioned above, the composite scaffold does not change its shape during the recovery period of SCI and does not damage the regenerated nerve. Therefore, as an implantable biocomposite material, it has broad application prospects in SCI.

In addition to its good mechanical properties, the scaffold retained the basement layer in the HAM. Previous studies have shown that the mechanical properties and tensile strength of the HAM are guaranteed by the basement membrane layer. As the ECM on which human amniotic epithelial cells (hAECs) adhere, the basement membrane contains HA and various basal proteins, such as collagen types I to IV, laminin-1, laminin-5, and fibronectin, which ensure hAEC differentiation, proliferation, and migration. HA and various basal proteins can support nerve repair after SCI [39]. Liang et al. demonstrated the role of the matrix in promoting axon regeneration and repairing SCI [12], which is the same as our conclusion. GelMA–HAAMMA can strengthen newborn neuron growth after injury [40].

After the occurrence of SCI, the factors affecting healing are often dominated by fibrous and glial scars. Extensive fibrous scar production usually results in wound deformation, tearing, and void formation. Thus, it affects tissue healing. Glial scars, dominated by astrocytes, affect the passage of new nerve axons, leading to difficulties in nerve regeneration. Results of the in vivo animal experiments showed that the tissue healing and nerve regeneration abilities of the GelMA–HAAMMA group were better than those of the other groups, which confirmed our findings. An interesting phenomenon occurred in the GelMA–HAAMMA group, which showed that when neurons were regenerated, many astrocytes were also generated. It was hypothesized that abundant collagen and biological factors may promote astrocyte generation at the early stage of HAAM attachment to the spinal cord [29, 33]. The bilayer crossing structure of the composite scaffold may avoid the effect of astrocytes on neuronal regeneration. This phenomenon needs to be further studied. The degradation rate of GelMA–HAAMMA was not significantly improved compared to that of GelMA. To play a further role in SCI recovery, HAAM needs to be further modified in subsequent studies.

Perfect materials do not exist in SCI-related tissue engineering research. The materials designed by the researchers are made from different raw materials and have a wide range of ingredients. However, the ultimate goal of all composites is to promote central nerves regeneration. In an ideal scaffold, the newly formed axons can overcome various obstacles to pass through the injured area of SCI, resulting in the recovery of sensory and motor functions. After ensuring such an effect, further optimization of the composite can proceed. The GelMA–HAAMMA composite scaffold discussed in this study is a successful first step. Future research will search for bioengineering materials with better scar treatment effects and longer degradation time to ensure the therapeutic effect and promote the research of SCI recovery.

Conclusions

In this study, HAAM and MA were chemically grafted to form HAAMMA, which was subsequently photocrosslinked with GelMA gel to prepare the GelMA–HAAMMA composite scaffold. During coculture with neurons, there was no change in cell survival after three days of coculture with GelMA–HAAMMA. In the HUVEC proliferation assay, the healing effect of the GelMA–HAAMMA group was the most obvious. In the in vitro angiogenesis assay, the number of new blood vessels in the GelMA–HAAMMA group was the highest. This study confirmed that composite scaffolds can be prepared quickly and that their biological activity was not destroyed. GelMA–HAAMMA not only possesses the excellent mechanical properties of GelMA but also retains the good biocompatibility and low immunogenicity of HAAM. It is a bioactive material for tissue engineering. In the animal experiment, the spinal cord homeostasis of SD rats treated with GelMA–HAAMMA was the best. They also had the higher number of new neurons than any other group (except for sham). In the assessment of motor function recovery, rats in the GelMA–HAAMMA group also achieved the highest BBB scores. Composite scaffolds can effectively construct the extracellular environment in SCI, regulate pathological changes, and promote the generation of new neurons. Rats treated with the composites showed significant recovery of motor function after the operation. Therefore,

GelMA–HAAMMA is a promising biocomposite material for central nerves repair after SCI.

Supplementary Information The online version contains supplementary material available at https://doi.org/10.1007/s42242-024-00318-x.

Acknowledgements This work was supported by the National Natural Science Foundation of China (No. 82371383). All the authors appreciate the efforts of the Department of Obstetrics, Affiliated Hospital of Nantong University for donating human amniotic membrane and human umbilical vein endothelial cells.

Author contributions TX was responsible for the design of the experimental procedure, verified the composite material, participated in the whole process of experiments and wrote the article, and was the main contributor. CWY and YL were responsible for the preparation and validation of acellular amniotic membrane and the design of in vitro animal experiments. HW was responsible for photographing the in vitro cell experiments. CC was responsible for data collection for the in vitro experiments. YCZ was responsible for all data integration and collating. XQC was responsible for reviewing the correctness of the experimental design, the rigor of the experimental verification, and the final review of the paper.

Availability of data and material Data will be made available on request. TX is responsible for receiving contact to provide relevant data.

Declarations

Conflict of interest The authors declare that they have no conflict of interest.

Ethical approval All experimental procedures were performed in accordance with the Guide for the Care and Use of Laboratory Animals of the National Research Council. The animal ethics approval was approved by the Animal Care and Use Committee of Nantong University (Nantong, China; 220203322/22020214810).

References

1. Paolin A, Trojan D, Leonardi A et al (2016) Cytokine expression and ultrastructural alterations in fresh-frozen, freeze-dried and gamma-irradiated human amniotic membranes. Cell Tissue Bank 17(3):399–406. https://doi.org/10.1007/s10561-016-9553-x
2. Wang MG, Yang S, Cao Z et al (2020) Application of acellular tissue matrix for enhancement of weak abdominal wall in animal model. BioMed Res Int 2020:3475289. https://doi.org/10.1155/2020/3475289
3. Wilshaw SP, Kearney J, Fisher J et al (2008) Biocompatibility and potential of acellular human amniotic membrane to support the attachment and proliferation of allogeneic cells. Tissue Eng Pt A 14(4):463–472. https://doi.org/10.1089/tea.2007.0145
4. Abazari MF, Soleimanifar F, Enderami SE et al (2020) Decellularized amniotic membrane scaffolds improve differentiation of iPSCs to functional hepatocyte-like cells. J Cell Biochem 121(2):1169–1181. https://doi.org/10.1002/jcb.29351
5. Murphy SV, Skardal A, Song LJ et al (2017) Solubilized amnion membrane hyaluronic acid hydrogel accelerates full-thickness wound healing. Stem Cells Transl Med 6(11):2020–2032. https://doi.org/10.1002/sctm.17-0053
6. Nouri M, Ebrahimi M, Bagheri T et al (2018) Healing effects of dried and acellular human amniotic membrane and mepitelas for coverage of skin graft donor areas; a randomized clinical trial. Bull Emerg Trauma 6(3):195–200
7. Gholipourmalekabadi M, Bandehpour M, Mozafari M et al (2015) Decellularized human amniotic membrane: more is needed for an efficient dressing for protection of burns against antibiotic-resistant bacteria isolated from burn patients. Burns 41(7):1488–1497. https://doi.org/10.1016/j.burns.2015.04.015
8. Salah RA, Mohamed IK, El-Badri N (2018) Development of decellularized amniotic membrane as a bioscaffold for bone marrow-derived mesenchymal stem cells: ultrastructural study. J Mol Histol 49(3):289–301. https://doi.org/10.1007/s10735-018-9768-1
9. Higa K, Shimmura S, Shimazaki J et al (2005) Hyaluronic acid-CD44 interaction mediates the adhesion of lymphocytes by amniotic membrane stroma. Cornea 24(2):206–212. https://doi.org/10.1097/01.ico.0000133999.45262.83
10. Xiao SN, Xiao CF, Miao Y et al (2021) Human acellular amniotic membrane incorporating exosomes from adipose-derived mesenchymal stem cells promotes diabetic wound healing. Stem Cell Res Ther 12(1):255. https://doi.org/10.1186/s13287-021-02333-6
11. Mligiliche N, Endo K, Okamoto K et al (2002) Extracellular matrix of human amnion manufactured into tubes as conduits for peripheral nerve regeneration. J Biomed Mater Res 63(5):591–600. https://doi.org/10.1002/jbm.10349
12. Liang HS, Liang P, Xu Y et al (2009) DHAM-BMSC matrix promotes axonal regeneration and functional recovery after spinal cord injury in adult rats. J Neurotrauma 26(10):1745–1757. https://doi.org/10.1089/neu.2008.0850
13. Kim W, Lee H, Lee J et al (2020) Efficient myotube formation in 3D bioprinted tissue construct by biochemical and topographical cues. Biomaterials 230:119632. https://doi.org/10.1016/j.biomaterials.2019.119632
14. Lei XY, Wu YC, Peng X et al (2020) Research on alginate-polyacrylamide enhanced amnion hydrogel, a potential vascular substitute material. Mater Sci Eng C 115:111145. https://doi.org/10.1016/j.msec.2020.111145
15. Annabi N, Mithieux SM, Zorlutuna P et al (2013) Engineered cell-laden human protein-based elastomer. Biomaterials 34(22):5496–5505. https://doi.org/10.1016/j.biomaterials.2013.03.076
16. Annabi N, Rana D, Sani ES et al (2017) Engineering a sprayable and elastic hydrogel adhesive with antimicrobial properties for wound healing. Biomaterials 139:229–243. https://doi.org/10.1016/j.biomaterials.2017.05.011
17. Zhang Q, Chang CW, Qian CY et al (2021) Photo-crosslinkable amniotic membrane hydrogel for skin defect healing. Acta Biomater 125:197–207. https://doi.org/10.1016/j.actbio.2021.02.043
18. Gholipourmalekabadi M, Samadikuchaksarae A, Seifalian AM et al (2018) Silk fibroin/amniotic membrane 3D bi-layered artificial skin. Biomed Mater 13(3):035003. https://doi.org/10.1088/1748-605X/aa999b
19. Zhang Q, Qian CY, Xiao WS et al (2019) Development of a visible light, cross-linked GelMA hydrogel containing decellularized human amniotic particles as a soft tissue replacement for oral mucosa repair. RSC Adv 9(32):18344–18352. https://doi.org/10.1039/c9ra03009c
20. Zhao X, Lang Q, Yildirimer L et al (2016) Photocrosslinkable gelatin hydrogel for epidermal tissue engineering. Adv Healthc Mater 5(1):108–118. https://doi.org/10.1002/adhm.201500005
21. Sang SB, Yan YY, Shen ZZ et al (2022) Photo-crosslinked hydrogels for tissue engineering of corneal epithelium. Exp Eye Res 218:109027. https://doi.org/10.1016/j.exer.2022.109027
22. Ma DHK, Lai JY, Cheng HY et al (2010) Carbodiimide cross-linked amniotic membranes for cultivation of limbal epithelial cells. Biomaterials 31(25):6647–6658. https://doi.org/10.1016/j.biomaterials.2010.05.034

23. Gage FH, Blaker SN, Davis GE et al (1988) Human amnion membrane matrix as a substratum for axonal regeneration in the central nervous system. Exp Brain Res 72(2):371–380. https://doi.org/10.1007/BF00250258
24. Kshersagar J, Kshirsagar R, Desai S et al (2018) Decellularized amnion scaffold with activated PRP: a new paradigm dressing material for burn wound healing. Cell Tissue Bank 19(3):423–436. https://doi.org/10.1007/s10561-018-9688-z
25. Wang H, Tang Q, Lu Y et al (2023) Berberine-loaded MSC-derived sEVs encapsulated in injectable GelMA hydrogel for spinal cord injury repair. Int J Pharmaceut 643:123283. https://doi.org/10.1016/j.ijpharm.2023.123283
26. Bankiewicz KS, Palmatier M, Plunkett RJ et al (1994) Reversal of hemiparkinsonian syndrome in nonhuman primates by amnion implantation into caudate nucleus. J Neurosurg 81(6):869–876. https://doi.org/10.3171/jns.1994.81.6.0869
27. Bajpai I, Kim DY, Kyong-Jin J et al (2017) Response of human bone marrow-derived MSCs on triphasic Ca-P substrate with various HA/TCP ratio. J Biomed Mater Res B 105(1):72–80. https://doi.org/10.1002/jbm.b.33538
28. Yang YM, Fan YH, Zhang HP et al (2021) Small molecules combined with collagen hydrogel direct neurogenesis and migration of neural stem cells after spinal cord injury. Biomaterials 269:120479. https://doi.org/10.1016/j.biomaterials.2020.120479
29. Liu XZ, Zhang LL, Xu ZJ et al (2022) A functionalized collagen-I scaffold delivers microRNA 21-loaded exosomes for spinal cord injury repair. Acta Biomater 154:385–400. https://doi.org/10.1016/j.actbio.2022.10.027
30. Wu ZP, Liu XY, Yuan D et al (2018) Human acellular amniotic membrane is adopted to treat venous ulcers. Exp Ther Med 16(2):1285–1289. https://doi.org/10.3892/etm.2018.6331
31. Mohammad J, Shenaq J, Rabinovsky E et al (2000) Modulation of peripheral nerve regeneration: a tissue-engineering approach. The role of amnion tube nerve conduit across a 1-centimeter nerve gap. Plast Reconstr Surg 105(2):660–666. https://doi.org/10.1097/00006534-200002000-00027
32. Liu XY, Hao MM, Chen ZJ et al (2021) 3D bioprinted neural tissue constructs for spinal cord injury repair. Biomaterials 272:120771. https://doi.org/10.1016/j.biomaterials.2021.120771
33. Shen H, Xu B, Yang C et al (2022) A DAMP-scavenging, IL-10-releasing hydrogel promotes neural regeneration and motor function recovery after spinal cord injury. Biomaterials 280:121279. https://doi.org/10.1016/j.biomaterials.2021.121279
34. Sadraie SH, Parivar K, Arabi F et al (2016) Study of transected sciatic nerve repair by amniotic membrane with betamethasone in adult albino Wistar rats. Arch Iran Med 19(9):612–617
35. Clayman GL, Roy R, Norman J (2022) Human amnion/chorion membrane may reduce transient recurrent laryngeal nerve injury during thyroid surgery. Cell Transplant 31:09636897211073136. https://doi.org/10.1177/09636897211073136
36. Yue K, Trujillo-de Santiago G, Alvarez MM et al (2015) Synthesis, properties, and biomedical applications of gelatin methacryloyl (GelMA) hydrogels. Biomaterials 73:254–271. https://doi.org/10.1016/j.biomaterials.2015.08.045
37. Fan CX, Yang W, Zhang LL et al (2022) Restoration of spinal cord biophysical microenvironment for enhancing tissue repair by injury-responsive smart hydrogel. Biomaterials 288:121689. https://doi.org/10.1016/j.biomaterials.2022.121689
38. Noor N, Shapira A, Edri R et al (2019) 3D printing of personalized thick and perfusable cardiac patches and hearts. Adv Sci 6(11):1900344. https://doi.org/10.1002/advs.201900344
39. Choudhury D, Tun HW, Wang TY et al (2018) Organ-derived decellularized extracellular matrix: a game changer for bioink manufacturing? Trends Biotechnol 36(8):787–805. https://doi.org/10.1016/j.tibtech.2018.03.003
40. Mohammad JA, Warnke PH, Pan YC et al (2000) Increased axonal regeneration through a biodegradable amnionic tube nerve conduit: effect of local delivery and incorporation of nerve growth factor/hyaluronic acid media. Ann Plast Surg 44(1):59–64. https://doi.org/10.1097/00000637-200044010-00010